The Stirring Tropics. Part II: Theory of Moisture Mode–Hadley Cell Interactions

Ángel F. Adames Corraliza , Víctor C. Mayta

Department of Atmospheric and Oceanic Sciences, University of Wisconsin, Madison, Wisconsin

This manuscript was submitted on 03/13/2023 and has not been peer-reviewed.

ABSTRACT: Interactions between large-scale waves and the Hadley Cell are examined using a linear two-layer model on an f-plane. A linear meridional moisture gradient determines the strength of the idealized Hadley Cell. The trade winds are in thermal wind balance with a weak temperature gradient (WTG). The mean meridional moisture gradient is unstable to moisture modes that are advected westward by the trade winds. Meridional moisture advection causes the moisture modes to grow from "moisture-vortex instability" (MVI), resulting in a poleward eddy moisture flux that flattens the meridional moisture gradient, thereby weakening the Hadley Cell. The resulting Hadley Cell-moisture mode interaction is reminiscent of quasi-geostrophic interactions, except that wave activity is due to column moisture variance rather than potential vorticity variance. WTG balance reduces the Lorenz energy cycle to the kinetic energy budget. The conversion of zonal mean kinetic energy to eddy kinetic energy is due to the poleward eddy moisture flux and hence the tendency in wave activity. These conversions are maintained in steady state via continuous regeneration of the meridional moisture gradient by the Hadley Cell, and eddy moisture diffusion, implying a downscale latent energy cascade in the tropics. It is proposed that moisture modes are the tropical analog to midlatitude baroclinic waves. MVI is analogous to baroclinic instability, stirring latent energy in the same way that dry baroclinic eddies stir sensible heat. These results indicate that moisture modes stabilize the Hadley Cell and may be as important as the latter in the global energy transport.

SIGNIFICANCE STATEMENT: The tropics are characterized by steady circulations such as the Hadley Cell as well as a menagerie of weather systems such as tropical waves. Despite progress in our understanding of both, little is known about how the mean circulations and the tropical waves interact with one another. Here we show that tropical waves grow by extracting moisture from the Hadley Cell, thereby weakening it. They also transport moisture to higher latitudes. Our results challenge the notion that the Hadley Cell is the sole transporter of energy out of the tropics and instead favor a view where tropical waves are also essential for the global energy balance. They dry the humid regions and moisten the drier regions via stirring.

1. Introduction

Prior the second world war, many atmospheric scientists believed the tropics to be very stable outside of the occasional occurrence of tropical cyclones (see prologue in Riehl 1954). As interest in the tropics grew and observations increased, scientists showed that the tropics contain a diversity of "tropical weather systems" that exhibit a wide variety of spatial and temporal scales. Near the equator, studies have documented the existence of convectively-coupled equatorial waves (Matsuno 1966; Kiladis et al. 2009), and the Madden-Julian Oscillation (Madden and Julian 1972). Away from the equator, we see tropical cyclones and a variety of tropical depression-like (TD-like) systems that include monsoon low-pressure systems and easterly waves (Riehl 1954; Chang 1970; Mooley 1973)

Interestingly, such a diversity of systems exists within an atmosphere that exhibits little spatial and temporal variations in temperature (Charney 1963), leading to the development of the weak temperature gradient (WTG) approximation (Sobel and Bretherton 2000; Sobel et al. 2001). They also coexist with the mean circulations: the Hadley and Walker Cells, and the monsoons.

Analysis of the governing thermodynamics of these systems has indicated that tropical weather systems exist in a spectrum (Adames et al. 2019; Inoue et al. 2020; Adames and Maloney 2021; Mayta and Adames 2023). Systems that propagate quickly exhibit thermodynamics that are governed by temperature fluctuations, as in gravity waves (Raymond et al. 2007; Herman et al. 2016). These are the systems that are responsible for maintaining WTG balance over the tropics (Bretherton and Smolarkiewicz 1989; Wolding et al. 2016; Adames and Maloney 2021). Slower-evolving convectively-coupled systems are often in WTG balance and their thermodynamics are governed by moisture, hence their name "moisture modes" (Yu and Neelin 1994; Raymond and Fuchs 2009; Adames and Maloney 2021).

Initially, only the MJO was hypothesized to be a moisture mode (Raymond and Fuchs 2009; Sugiyama 2009; Sobel and Maloney 2013). Numerous advances in our understanding of the MJO have resulted from its study under the moisture mode lens (see reviews by Zhang et al. 2020, Jiang et al. 2020 and Adames et al. 2021). While the idea of the MJO being a moisture mode remains a topic of debate

Corresponding author: Ángel F. Adames Corraliza, angel.adamescorraliza@wisc.edu

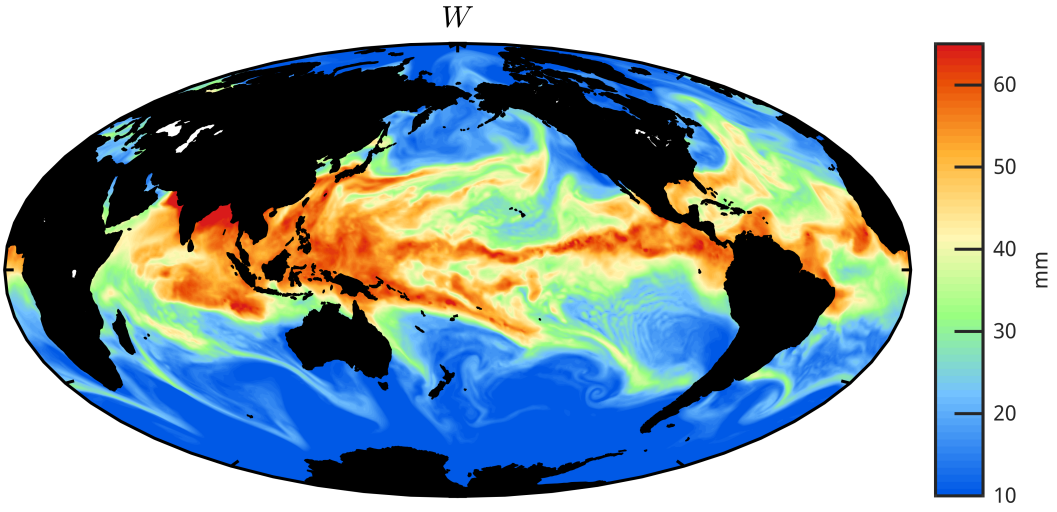

FIG. 1. Snapshot of ERA5 column-integrated water vapor W for June 29, 2017. Lands are masked out to emphasize the wavy behavior over the oceans.

(Powell 2017; Chen 2022a; Mayta and Adames-Corraliza 2023), other studies have indicated that moisture modes may be a broader feature of the tropics (Adames 2022; Inoue et al. 2020; Maithel and Back 2022; Mayta and Adames 2023). On the basis of scale analysis, Adames et al. (2019); Adames (2022) showed that systems with propagation speeds near 5 m s^{-1} are likely to be moisture modes. Such systems include most "rotational" tropical systems such as convectively-coupled equatorial Rossby waves and tropical depression-like systems.

Over the western hemisphere, observations indicate equatorial Rossby waves and TD-like waves are moisture modes (Mayta et al. 2022; Mayta and Adames 2023). The same results were identified over the eastern and western Pacific and over the Indian Ocean (Gonzalez and Jiang 2019; Nakamura and Takayabu 2022a,b; Chen 2022b; Mayta and Adames Corraliza 2023). Only African easterly waves do not fully exhibit moisture mode properties (Wolding et al. 2020; Núñez Ocasio and Rios-Berrios 2023). Wavenumber-frequency analysis also supports this hypothesis (Inoue et al. 2020). Storm-permitting simulations on an aquaplanet also reveal a high variance of moisture mode-like behavior in the form of easterly waves (Rios-Berrios et al. 2023). More recently, Maithel and Back (2022) found that convective recharge-discharge cycles can be explained well if these are assumed to behave like moisture modes. All these results allude to the potential commonality of moisture modes and the possibility of moisture mode theory to explain the behavior of organized tropical deep convection.

In spite of their geographical and structural differences, all these moisture modes are driven by the same processes. Their moist static energy (MSE) anomalies are governed by moisture and they propagate westward via horizontal moisture advection (Yasunaga et al. 2019; Inoue et al. 2020; Mayta and Adames Corraliza 2023). Many studies have shown that vertical MSE advection dissipates the systems, canceled by longwave radiative heating (Andersen and Kuang 2012; Sobel et al. 2014; Mayta et al. 2022). A less documented feature of these systems is that the advection of background-mean MSE by the anomalous meridional winds also contributes to the growth of these systems (Mayta and Adames Corraliza 2023). This type of growth was initially documented in the balanced moisture waves of Sobel et al. (2001) and was later coined by Adames and Ming (2018) as "moisture-vortex instability". While this instability was initially posited to explain the growth of monsoon low-pressure systems (Adames and Ming 2018), a companion study (Mayta and Adames Corraliza 2023) (part I henceforth) suggests that this mechanism is present in TD-like waves and equatorial Rossby waves over the globe. Furthermore, all the systems had the common feature that they are advected westward by the mean trade winds.

We hypothesize that the self-similarity of these balanced waves may be a fundamental feature of their interaction with the tropical mean state. This hypothesis is further strengthened by examining snapshots of column-integrated water vapor (Fig 1). In it, we see that the humid regions of the tropics appear wavy, even when there is no obvious sign of extratropical forcing. This large-scale behavior hints at the possibility that tropical waves may actively "stir" column water vapor, mixing it throughout the tropics. Observational support for this hypothesis already exists. Sherwood (1996) and (Pierrehumbert 1998) showed that the subtropics can moisten by horizontal transports of water vapor from the convecting regions. Conversely, many studies have shown that tongues of dry subtropical

air can intrude into the rainy regions of the tropics, suppressing rainfall (Mapes and Zuidema 1996; Parsons et al. 2000; Jensen and Del Genio 2006; Kerns and Chen 2014). Recently, Inoue et al. (2021) found that horizontal moisture advection is the primary cause of precipitation variability in the tropics. Furthermore, analysis of the poleward energy transport in the tropics shows a non-negligible poleward latent energy transport by transients at the sub-monthly timescale (Trenberth and Stepaniak 2003; Rios-Berrios et al. 2020), suggesting that this stirring is also important for the global energy balance. In part I, we showed that a statistically-significant signal in poleward moisture transport exists in westward-propagating moisture modes.

The putative similarity of moisture modes across the tropics becomes more intriguing when we compare them to unstable baroclinic waves. One of the main features of dry baroclinic instability is that they grow from meridional temperature advection. The phasing between meridional winds and the temperature anomalies causes the growing waves to exhibit a poleward heat flux, a major piece of midlatitude wave-mean flow interactions as crystalized in the Eliassen-Palm formulation of wave activity (Andrews and Mcintyre 1976; Edmon Jr et al. 1980). The heat flux acts to weaken the horizontal temperature gradient, therefore weakening the jet stream via thermal wind balance. If not for these fluxes, the temperature difference between the tropics and the globe would be much larger than observed.

This study aims to examine the possibility that an analogous wave-mean flow interaction exists in the tropics. In this analogy the moisture modes are akin to the baroclinic waves, interacting with the mean state via moisture advection rather than temperature advection. The Hadley Cell is the analog of the midlatitude jet stream. As in baroclinic instability, we hypothesize that *moisture modes grow by extracting energy from the mean meridional moisture gradient (i.e., MVI), flattening it and therefore weakening the Hadley Cell.*

In order to test this hypothesis, we will employ a simple two-layer model to examine how an idealized circulation could lead to the existence of moisture modes (Section 2). Then, we will examine the properties of these waves, including their propagation and growth (Section 3). Interactions between moisture modes and the Hadley Cell are discussed in Section 4. A concluding discussion about the main findings of this study is offered in Section 5.

2. Two-layer model

a. Model setup

We will use the two-layer model of Adames (2021) (A21 henceforth), which is the same model shown in Holton and Hakim (2012) except modified to include a prognostic moisture equation. This model allows us to include the effects of vertical wind shear but is also sufficiently simple to allow for a tractable analysis of its wave solutions. The main variables in this study are shown in Table 1 and constants with their values are shown in Table 2.

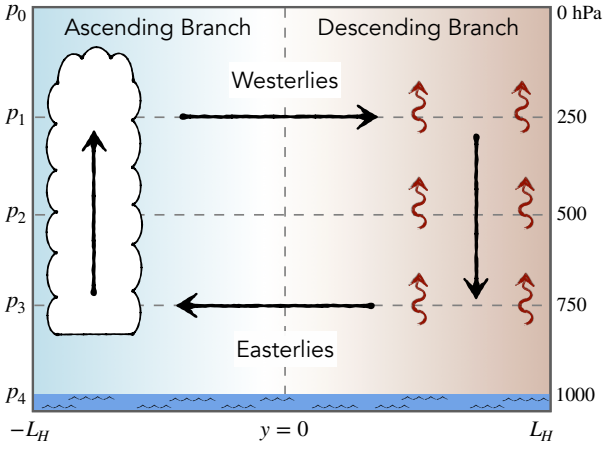

FIG. 2. Schematic describing the two-layer moist model used in this study. The arrows depict the direction of the overturning circulation. Blue shading indicates the humid ascending and brown indicates the dry, subsiding branch. Pressure levels in the model are shown on the left and their values are shown on the right. The cloud indicates the region of convective heating and the curly arrows indicate the radiative cooling.

TABLE 1. The main variables and definitions used in this study.

Var.	*Description*	*Units*
ψ	Streamfuction	$m^2\ s^{-1}$
Φ	Geopotential	$m^2\ s^{-2}$
T	Temperature	K
$\mathbf{v}$	Horizontal wind vector	$m\ s^{-1}$
ω	Vertical pressure velocity	$Pa\ s^{-1}$
ζ	Relative vorticity	s^{-1}
δ	Horizontal divergence	s^{-1}
P	Precipitation rate	Jkg^{-1}
E	Evaporation rate	Jkg^{-1}
R_{cs}	Clear-sky radiative cooling rate	Jkg^{-1}
r	Cloud-radiative feedback parameter	-
q	Specific humidity	-
W	Column-integrated moisture	mm
S	Gross dry stability	$J\ m^{-2}$
τ_c	Conv. moisture adjustment timescale	s
β_q	Mean meridional moisture gradient	$m^{-1}\ s^{-1}$
ϖ	Wave frequency	s^{-1}
k	Zonal wavenumber	m^{-1}
l	Meridional wavenumber	m^{-1}
K	Horizontal wavenumber	m^{-1}
KE	Integrated kinetic energy	$J\ m^{-1}$
APE	Available potential energy	$J\ m^{-1}$
ALE	Available latent energy	$J\ m^{-1}$
$\mathcal{A}$	Moisture mode activity	$J\ m^{-1}$

TABLE 2. Constants and their values.

Var.	*Description*	*Units*
C_p	Specific heat at constant pressure	1004 J kg^{-1} K^{-1}
R_d	Dry gas constant	287 J kg^{-1} K^{-1}
L_v	Latent heat of vaporization	2.5×10^6 J kg^{-1}
L_H	Hadley Cell half width	1000 km
Δp	Atmosphere half depth	500 hPa
f_0	Planetary vorticity	3×10^{-5} s^{-1}
S	Gross dry stability	1.3×10^8 J m^{-2}
c	Free gravity wave phase speed	58 m s^{-1}
L_d	Rossby radius of deformation	2×10^6 m
ϵ	Dissipation coefficient	0.75×10^{-6} s^{-1}
τ_c	Domain-mean convective moisture adjustment timescale	10 days
$L_v[\overline{E}]$	Domain-mean latent heat flux	100 W m^{-2}
R_{cs}	Column radiative cooling rate	110 W m^{-2}
$[\overline{W}]$	Domain-mean column moisture	40 kg m^{-2}
l	First meridional wavenumber	1.5×10^{-6} m^{-1}
β_q	Mean meridional moisture gradient (in units of vorticity gradient)	1×10^{-11} (m s)$^{-1}$

We will modify the model of A21 to account for the presence of an idealized Hadley Cell, and examine motions under the WTG approximation, rather than the quasi-geostrophic approximation. The layout of the model is shown schematically in Fig. 2. The idealized Hadley Cell is comprised of equatorward and easterly winds in the lower troposphere and poleward and westerly winds in the upper troposphere. The equatorward side of Cell is ascending and humid, while the poleward side is descending and dry. Since we are interested in understanding the interactions between waves and the Hadley Cell in isolation, we will bind our model with rigid lids at a distance L_H from the center of the domain.

As in A21, we will assume that the vertical velocity (ω) attains a maximum amplitude in layer 2, and becomes zero at the top and bottom boundaries. For simplicity, we assume that ω increases linearly from p_0 to p_2, and decreases linearly thereafter. As a result, ω_3 can be written in terms of ω_2 as:

$$\omega_1 = \omega_3 = \frac{\omega_2}{2}. \tag{1}$$

By assuming that ω has a simple structure, we can invoke mass continuity in each discrete layer in order to relate it to the horizontal divergence (δ). Hence, we can write the divergence in layers 1 and 3 as:

$$\delta_3 = \frac{\omega_2}{\Delta p} \qquad \delta_1 = -\delta_3 \tag{2}$$

where Δp is half the depth of the atmosphere in this model.

Many of the variables used here will be column integrated and/or zonally averaged or meridionally-integrated. For any variable X, these operations are defined as:

$$\langle X \rangle = \frac{1}{g}\int_{p_0}^{p_4} X dp \tag{3a}$$

$$\overline{X} = \frac{1}{2\pi a \cos\varphi}\oint X dx \tag{3b}$$

$$[X] = \int_{-L_H}^{L_H} X dy \tag{3c}$$

where $a = 6378$ km is the radius of the Earth, and $\varphi = 13°$N is our reference latitude. Deviations from this zonal average will be denoted as primes, i.e:

$$X' = X - \overline{X}. \tag{4}$$

The column integration will allow us to represent the apparent heating and moisture sink, Q_1 and Q_2 respectively, in terms of surface processes and column radiative heating. Following Yanai et al. (1973), we can column integrate Q_1 and Q_2, yielding:

$$\langle Q_1 \rangle = L_v P + \langle Q_r \rangle \tag{5}$$

$$\langle Q_2 \rangle = L_v (P - E) \tag{6}$$

where P is the surface precipitation rate, E is the surface evaporation, and $\langle Q_r \rangle$ is the column radiative heating rate. The $\langle Q_r \rangle$ is decomposed into a cloud-radiative heating component and a clear-sky radiative cooling R_{cs}:

$$\langle Q_r \rangle = r L_v P - R_{cs} \tag{7}$$

where r is the cloud-radiative feedback parameter (Peters and Bretherton 2005) or the greenhouse enhancement factor (Kim et al. 2015). Note that the effect of water vapor on radiative heating is implicitly included in r.

Precipitation is coupled with column-integrated water vapor ($W = \langle q \rangle$, where q is the specific humidity) in the lower troposphere via a linear relaxation time:

$$P = \frac{W}{\tau_c} \tag{8}$$

where τ_c is a convective moisture relaxation timescale. While the relationship between P and W is nonlinear (Bretherton et al. 2004; Ahmed and Neelin 2018; Ahmed et al. 2020; Emanuel 2019), using this linear form will significantly simplify the interpretation of the results of this study.

b. Domain means

Let us assume that our domain is in radiative-convective equilibrium (Manabe and Strickler 1964) and has a balanced hydrologic cycle. As a result, the globally-averaged balances in the thermodynamic and moisture equations are:

$$L_v[\overline{P}](1+r) = R_{cs} \tag{9a}$$

$$[\overline{P}] = [\overline{E}]. \tag{9b}$$

Given that $L_v[\overline{P}] \sim 100$ W m^{-2} yields a radiative cooling rate of ~ 110 W m^{-2}, assuming that $r = 0.1$.

The constraints on the global hydrologic cycle also constrain the global-mean value of τ_c to $[\overline{W}]/[\overline{P}]$. With tropical-mean values of $[\overline{W}] = 40$ mm we obtain a value of τ_c of ~ 10 days. This timescale is much larger than what empirical data suggests (Bretherton et al. 2004; Rushley et al. 2018; Adames et al. 2017). However, it is important to note that the τ_c is usually defined for regions of high precipitation, not for the tropical average. While the large and fixed value of τ_c is a limitation of this study, it will not affect the interpretation of the results.

We posit that the equatorward edge of the Hadley Cell has a lapse rate that is roughly a moist adiabat, as in Emanuel (2019). Because the domain is in WTG balance, gravity waves will transmit this lapse rate to the rest of the domain. Assuming that layer 0 is dry and that layer 4 roughly corresponds to the boundary layer, we find that the domain-mean vertical change in DSE is equal to the boundary layer latent energy evaluated at $-L_H$:

$$[s_0] - [s_4] = L_v q_4(-L_H) \tag{10}$$

where $s = C_p T + \Phi$ is the dry static energy, T is the temperature and Φ is the geopotential. If $W = q_3 \Delta p/g$ is 55 mm at $-L_H$, and approximating $q_4 \simeq 2q_3$, we find that $\overline{q}_4 \simeq 0.02$, a value often seen in deep tropical boundary layers (Ciesielski et al. 2003; de Szoeke 2018). Using this value we find that $\Delta s = 5 \times 10^4$ J kg^{-1}.

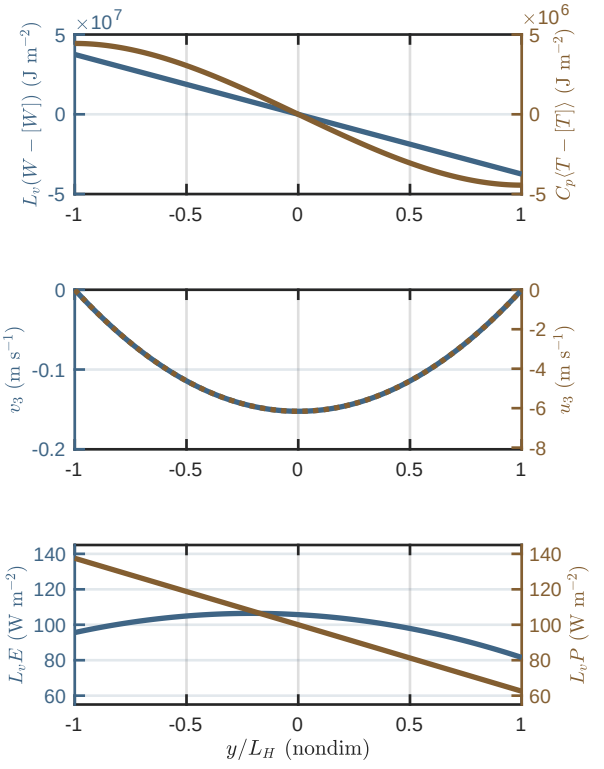

FIG. 3. (a) Meridional profile of $L_v(\overline{W} - [\overline{W}])$ (blue) and $C_p(\langle \overline{T} - [\overline{T}] \rangle)$ (brown), (b) $\overline{v}_3$ (blue) and $\overline{u}_3$ (brown), and (c) L_vE (blue) and L_vP (brown).

c. Zonal mean state

The rising and sinking branches of the Hadley Cell are determined by the values of $\overline{W}$, which is assumed to decrease linearly with increasing y:

$$\overline{W}(y) = [\overline{W}] + y\frac{\partial \overline{W}}{\partial y} \tag{11}$$

For reference, the meridional profile of $y\partial_y \overline{W}$ is shown in the top panel of Fig. 3.

We will assume that the Hadley Cell is approximately in WTG balance so that our zonal-mean thermodynamic balance is:

$$-\overline{\delta}_3 S = L_v \overline{P}(1+r) - R_{cs} \tag{12}$$

where

$$S = ([\overline{s}_0] - [\overline{s}_4])\frac{\Delta p}{2g} \tag{13}$$

is the gross dry stability, defined as in Yu et al. (1998) and treated here as a positive constant. Because we are assuming that the meridional mean moisture gradient is constant,

it follows that the mean divergence gradient must also be constant. By making use of Eq. (9a), and noting that $\overline{\delta}_3 = \partial_y \overline{v}_3$, we integrate Eq. (12) meridionally to obtain:

$$\overline{v}_3 = \overline{v}_0 \left(1 - \frac{y^2}{L_H^2}\right) \tag{14}$$

where L_H is the Hadley Cell half-width, assumed constant, and $\overline{v}_0$ is the meridional wind over the reference latitude:

$$\overline{v}_0 = \frac{L_H^2 (1+r)}{2S\tau_c} \frac{\partial L_v \overline{W}}{\partial y} \tag{15}$$

Assuming that $L_H \simeq 1000$ km, and $\partial_y \overline{W} = -15$ mm per 1000 km we obtain that $\overline{v}_0 = -0.2$ m s^{-1}. In Fig 3b we see that $\overline{v}_3$ is strongest over the reference latitude, and decreases to zero at $\pm L_H$.

We will assume that the horizontal momentum balance in the Hadley Cell is characterized by a balance between the Coriolis force and friction in the zonal momentum equation and geostrophic balance in the meridional momentum equation:

$$\epsilon \overline{u}_3 = f_0 \overline{v}_3 \tag{16a}$$

$$f_0 \overline{u}_3 = -\frac{\partial \Phi}{\partial y} \tag{16b}$$

where ϵ is a dissipation coefficient. Assuming that $\epsilon = 0.75 \times 10^{-6}$ s^{-1} we find that the mean zonal wind at the reference latitude is ~ 6 m s^{-1} (Fig. 3b).

By following Eqs. (12)-(16) but for layer 1, we find that the upper tropospheric winds are equal and opposite to the lower-tropospheric winds:

$$\overline{u}_1 = -\overline{u}_3 \tag{17a}$$

$$\overline{v}_1 = -\overline{v}_3 \tag{17b}$$

We can now use (17) to obtain the thermal wind relation, which takes the following form in this model:

$$\frac{\partial \overline{T}_2}{\partial y} = \frac{2 f_0}{R_d} \overline{u}_3. \tag{18}$$

Assuming that our Hadley Cell has a mean zonal wind of $\overline{u}_1 = -\overline{u}_3 = 6$ m s^{-1}, and using a reference latitude of 12°, we find that the mean meridional temperature gradient is on the order of ~ 1 K per 1000 km. When compared to the mean moisture gradient we see that the temperature gradient is roughly 9 times weaker (Fig. 3a). The small temperature gradient maintains the mean zonal winds but is sufficiently weak that it will allow us to employ the WTG approximation.

Lastly, in order to balance the moisture budget, we diagnose the mean surface evaporation as:

$$\overline{E} = \overline{P} + \frac{\partial \overline{v}_3 \overline{W}}{\partial y}. \tag{19}$$

The resulting meridional profile of $\overline{E}$ is nearly constant on the equatorward side of the Hadley Cell but shows a small decrease on the subsiding branch (Fig. 3c), qualitatively in agreement with observations (Fig. 5.2 of Hartmann 2015).

d. Simplified basic equations

We can substantially simplify the model of A21 if the following conditions are satisfied for the motions of interest. The conditions enumerated below come directly from the scaling of Adames (2022).

1. *Thermodynamic variations are in WTG balance.* For QG scaling, WTG balance is satisfied when:

$$\mathrm{N}_w = \frac{L_y^2}{L_d^2} \ll 1 \tag{20}$$

where L_y is the meridional scale of the system, and

$$L_d = \frac{c}{f_0} \qquad c = \left(\frac{R_d \Delta s}{2 C_p}\right)^{\frac{1}{2}} \tag{21}$$

where L_d is the Rossby deformation radius, and c is the gravity wave phase speed. As we will be shown below, the meridional scale of the motion is determined by L_H, and the largest value that L_y can take is $2L_H/\pi \sim 6.4 \times 10^5$ m. For the motions we are interested in we have that $\mathrm{N}_w \sim 0.1$.

2. *Moisture modes are the main synoptic-scale motion.* Adames (2022) showed that for motions to be considered moisture modes it is not sufficient for it to be in WTG balance. Rather, $L_v W$ must govern the distribution of anomalous column moist enthalpy ($L_v W' + C_p \langle T' \rangle$). A small value of N_{mode} implies that $L_v W' \gg C_p \langle T' \rangle$. Since we are considering motions at high moisture values, it is convenient to define N_mode following Adames et al. (2019)

$$\mathrm{N}_{mode} = \frac{L_x}{\overline{u}_3 \tau_c} \mathrm{N}_w \ll 1 \tag{22}$$

Plugging in all the defined values yields $\mathrm{N}_{mode} \sim 0.02$.

With the three conditions stated above, the basic equations in the two-layer model are written as:

$$\frac{\partial \zeta_1}{\partial t} = -\mathbf{v}_1 \cdot \nabla_h \zeta_1 - f_0 \delta_1 - \epsilon \zeta_1 \tag{23a}$$

$$\frac{\partial \zeta_3}{\partial t} = -\mathbf{v}_3 \cdot \boldsymbol{\nabla}_h \zeta_3 - f_0 \delta_3 - \epsilon \zeta_3 \tag{23b}$$

$$-\delta_3 S = L_v P (1+r) - R_{cs} \tag{23c}$$

$$\frac{\partial W}{\partial t} = -\boldsymbol{\nabla}_h \cdot (\mathbf{v}_3 W) - P + E \tag{23d}$$

where the numbered subscripts indicate the layer of the variable as indicated in Fig. 2.

When examining Eq. (23), we see that all the information necessary to understand the evolution of the system is contained in Eqs. (23b)-(23d). The upper-tropospheric vorticity does not play a role in the evolution of ζ_3 and W. Hence, we will drop it and note that it is still used to determine the vertical structure of the resulting waves. Thus, we can combine Eqs. (23b)-(23d) to obtain the following equations vorticity and moisture:

$$\frac{\partial \zeta_3}{\partial t} = -\mathbf{v}_3 \cdot \boldsymbol{\nabla}_h \zeta_3 - \frac{f_0}{S}\left(\frac{L_v W}{\tau_c}(1+r) - R_{cs}\right) - \epsilon \zeta_3 \tag{24a}$$

$$\frac{\partial W}{\partial t} = -\mathbf{v}_3 \cdot \boldsymbol{\nabla}_h W + C \tag{24b}$$

where

$$C = -\left(1 - \frac{L_v W}{S}(1+r)\right)\frac{W}{\tau_c} - \frac{W}{S} R_{cs} + E \tag{25}$$

is the so-called column process (Chikira 2014). It is worth noting that $L_v W/S$ is the so-called Chikira parameter α, while $1 - L_v W/S$ is equivalent to the so-called "gross moist stability" (Neelin and Held 1987). However, we opt to keep the current form since it shows that the first term on the rhs of Eq. (25) is quadratic in W.

3. Linear wave solutions

We will now linearize Eq. (24) with respect to the idealized Hadley Cell. Over the entirety of our idealized Hadley Cell $|\overline{u}| \gg |\overline{v}|$, allowing us to drop the advection by $\overline{v}$ in our equations so long as the meridional scale of our wave solutions is similar to or larger than its zonal scale ($L_y \geq L_x$). We have verified that this is indeed the case and that dropping $\overline{v}_3$ from our linearized system of equations does not affect our results.

We will also s replace $\overline{u}_3$ with its meridional-mean value ($[\overline{u}_3]$). This is done in order to obtain simpler results that are more amenable to discussion. We recognize that this assumption is a caveat of this study. However, we can assume that similar instabilities exist in more complicated mean states, as the results of part I indicate[1].

As in Sobel et al. (2001), we decompose the horizontal winds into its irrotational and non-divergent components. Assuming that the frequency of the wave relative to the mean flow is small compared to f_0, we can assume that the nondivergent wind is much stronger than the irrotational wind (Eq. 37 in Sobel et al. 2001). Thus, we can write the horizontal winds in terms of a streamfunction (ψ):

$$u \simeq -\frac{\partial \psi}{\partial y} \qquad v \simeq \frac{\partial \psi}{\partial x} \tag{26}$$

recalling that $\zeta = \nabla_h^2 \psi$.

Since we are dealing with small amplitude waves, it follows that perturbations in vorticity are much smaller than the planetary vorticity $\zeta \ll f_0$. As a result $|\zeta'|$ should be on the order of 10^{-6} s^{-1} or less. It follows that $|\delta'|$ should be on the order of 10^{-7} s^{-1}. After linearizing the thermodynamic equation:

$$-\delta_3' S = L_v P' (1+r) \tag{27}$$

we see that $L_v P'$ is on the order of 10 W m^{-2}. From this equation, it follows that W' is on the order of 4 mm.

When linearizing C, we find that the perturbation column process is written as:

$$L_v C' = -\frac{L_v W'}{\tau_c}\left(1 + \frac{\tau_c R_{cs}}{S} - 2\frac{L_v \overline{W}}{S}(1+r)\right) + L_v E' \tag{28}$$

An examination of the terms in parenthesis in Eq. (28) roughly cancel, so that the sum of the three terms is on the order of 10^{-1}. Since $L_v P' \sim 10$ W m^{-2}, it follows that the first term on the rhs of Eq. (28) is on the order of 1 W m^{-2}. Since $|\zeta'| \sim 10^{-6}$ s^{-1} and $L_x \sim 10^6$ m, it follows that $v' \sim 1$ m s^{-1}. We also demonstrate that LvE' is on the order of 1 W m^{-2} (see Appendix A). On the other hand, an examination of $v' \partial_y L_v \overline{W}$ indicates that the term is on the order of 10 W m^{-2}. Thus, we conclude that

$$L_v |C'| \ll -\left| v_3' \frac{\partial L_v \overline{W}}{\partial y} \right| \tag{29}$$

and C' will be dropped henceforth. We have verified that dropping this term does not affect the resulting wave solutions.

With these assumptions and approximations, our linearized system of equations is written as:

$$\frac{\partial \zeta_3'}{\partial t} = -[\overline{u}_3]\frac{\partial \zeta_3'}{\partial x} + \frac{f_0}{S}\frac{L_v W'}{\tau_c}(1+r) \tag{30a}$$

$$\frac{\partial W'}{\partial t} = -[\overline{u}_3]\frac{\partial W'}{\partial x} - v_3'\frac{\partial \overline{W}}{\partial y} \tag{30b}$$

This system is very similar to the one shown in Sobel et al. (2001). They differ in the fact that the waves are bounded by rigid lids at $\pm L_H$. Assuming $\psi \to 0$ at the boundaries we find that wave solutions take the following

[1] Simple models of baroclinic instability usually invoke a constant background zonal wind, even though generalizations of it have been done with more realistic background-mean states.

form:

$$\psi_3' = \hat{\psi}_3' \cos(ly) \exp(ikx - i\varpi t) \tag{31a}$$

$$W' = \hat{W}' \cos(ly) \exp(ikx - i\varpi t) \tag{31b}$$

where k is the zonal wavenumber, l is the meridional wavenumber, and ϖ is the angular frequency. The fields W' and ψ_3' are related by the polarization relation:

$$W' = \frac{k\partial_y \overline{W}}{\varpi - [\overline{u}_3]k} \psi_3' \tag{32}$$

Because rigid lids bound our domain at $\pm L_H$, it follows that the wave solutions have meridional structures that are restricted to oscillate an integer amount of times over twice the width of the Hadley Cell ($4L_H$). Thus, l is defined as:

$$l = \frac{(2\hat{l} - 1)\pi}{2L_H} \qquad \hat{l} = 1, 2, 3...$$

On the other hand, k is defined in terms of a recurrent boundary condition:

$$k = \frac{\hat{k}}{a\cos\varphi} \qquad \hat{k} = 1, 2, 3...$$

By assuming the wave solutions in Eq. (31) and substituting in Eq. (30) we obtain the dispersion relation

$$\varpi = [\overline{u}_3]k \pm \sqrt{\frac{i\beta_q k}{\tau_c K^2}} \tag{33a}$$

where $K^2 = k^2 + l^2$ is the horizontal wavenumber, and

$$\beta_q = -\frac{f_0}{S} \frac{\partial L_v \overline{W}}{\partial y} (1 + r) \tag{33b}$$

is the mean meridional moisture gradient, expressed in the same units as β to facilitate its interpretation. Note that this definition differs from that of A21 as it is multiplied by $L_v W(1+r)/S$.

The dispersion relation in Eq. (33a) has two wave solutions, with one of them being unstable, as shown in Fig. 4. Two opposing processes contribute to the propagation of the wave. The first is advection by the mean lower-tropospheric winds, which acts to propagate the system westward. The second is vortex stretching arising from meridional moisture advection, which acts to propagate the system eastward. From Fig. 4, we see that the latter process is dominant at small k. As k increases, the phase speed asymptotically approaches the $[\overline{u}_3]$ value of -4 m s^{-1}. One can also interpret the growing synoptic scale systems as propagating against the mean winds, as in midlatitude Rossby waves, but with the direction of motion being opposite to theirs.

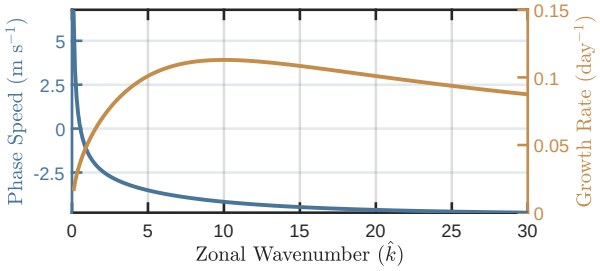

FIG. 4. Phase speed (blue) and growth rate (brown) of the unstable wave solution from Eq. (33).

Vortex stretching arising from meridional moisture advection is the only process that contributes to growth. Growth increases from wavenumber 1 and peaks near zonal wavenumber 10, decreasing afterward. It is worth pointing out that the instability is identical to the one that is obtained from Adames and Ming (2018) when their quadratic solution is not simplified. Thus, these systems grow from MVI. A close examination of Eq. (33a) shows that regardless of the sign of β_q, one of the wave solutions will always be unstable. Thus, *horizontal moisture gradients in the presence of rotation are always unstable*.

In Fig. 5 we see that the growing mode exhibits a horizontal structure that is mostly confined to the lower troposphere. Little signature is seen in the upper troposphere. The positive W and hence the P anomalies are shifted to the east of the center of low pressure (ψ' minimum). Because the P anomalies are shifted east of, but not in quadrature with ψ_3', it follows that the P anomalies are contributing to both the propagation and growth of the system, as Eq. (33a) indicates. In part I, we found that this phase relation is observed in many oceanic TD-like waves such as east Pacific easterly waves (Serra et al. 2008; Adames et al. 2022; Mayta and Adames 2023), all of which have moisture mode characteristics.

When examining the column-integrated moisture budget of the growing waves, which is equivalent to their MSE budget under WTG balance, we see that the fastest-growing zonal scale propagates westward nearly entirely from advection by the mean zonal winds and grows from meridional advection of mean moisture (Fig. 6), as was found for many TD-like and equatorial Rossby waves in part I.

4. Moisture mode-Hadley Cell interactions mediated by moisture transports

a. Moisture mode activity

We now return to the basic equations and consider interactions between the unstable wave solutions described in Eq. (33) and the mean state. As shown in Eq. (33)

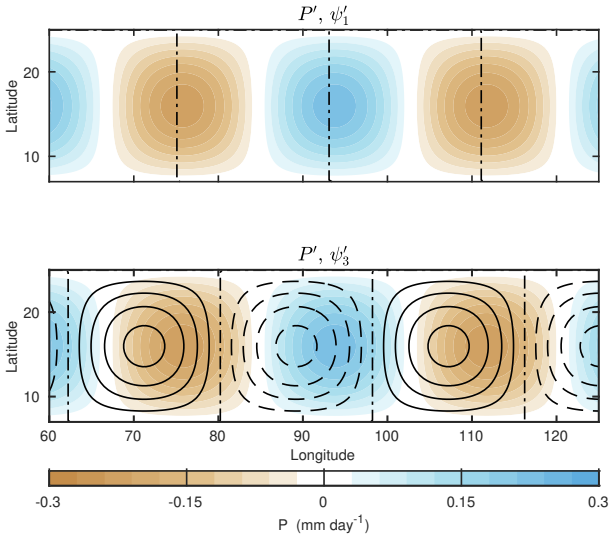

FIG. 5. Streamfunction anomalies of the growing wave solution from Eq. (33) in upper (layer 1, top) and lower troposphere (layer 3, bottom). The figure is constructed for zonal wavenumber 10 and the latitudes qualitatively represent the width of the Hadley Cell. The lower troposphere structure is obtained using Eq. (32). A similar procedure is used to obtain the upper-tropospheric structure. In both panels, P' is shown in shading. Contour interval 0.5×10^5 m^2 s^{-1}.

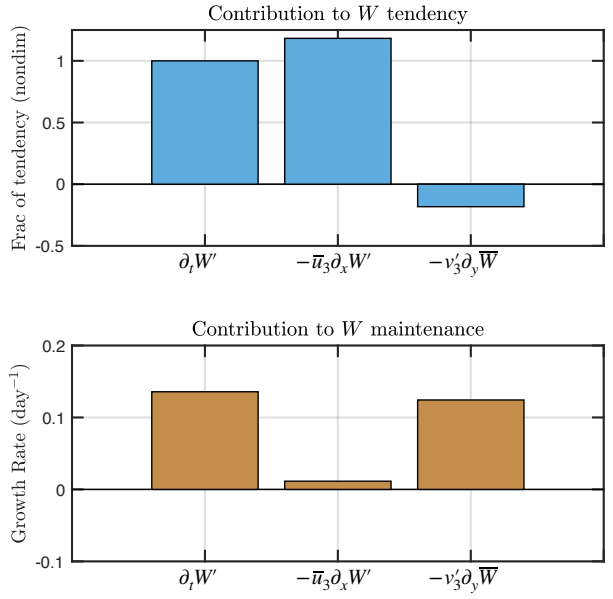

FIG. 6. Relative contribution of the two terms in Eq. (30b) to the (top) propagation and (bottom) growth of the W anomalies.

and Fig. 6, the growth of W' of the waves is largely determined by the meridional advection of $\overline{W}$ by v', a signature of MVI. This covariance between W' and v' will lead to increased moisture variance in the latitude band where the unstable waves are located. To elucidate this, we multiply Eq. (30b) by W' and zonally-average it. yielding a budget for the zonally-averaged column moisture variance:

$$\frac{1}{2}\frac{\partial \overline{W'^2}}{\partial t} = -\overline{v'W'}\frac{\partial \overline{W}}{\partial y}. \tag{34}$$

As suggested above, Eq. (34) shows that the moisture variance changes in time only when there is an eddy moisture flux downgradient of $\overline{W}$. A poleward flux of latent energy implies that MVI is occurring.

The presence of eddy moisture fluxes will induce a zonal-mean moisture tendency through its meridional divergence:

$$\frac{\partial \overline{W}}{\partial t} = -\frac{\partial \overline{v'W'}}{\partial y}. \tag{35}$$

When examining Eqs. (34) and (35) we see that the term $\overline{v'W'}$ appears in both equations, implying that $\overline{W}$ and W' are coupled. Furthermore, when comparing with QG theory, we can see that Eq. (34) resembles, and behaves similarly to the QG enstrophy equation, while Eq. (35) resembles the mean-state PV budget (Vallis 2017).

As in QG wave-mean flow interactions, we can use Eq. (34) to obtain an equation that describes the evolution of wave activity within our idealized Hadley Cell. By $\partial\overline{W}/\partial y$ and assuming that it varies in time much more slowly than $\overline{W'^2}$, we obtain the following:

$$\frac{\partial \mathcal{A}}{\partial t} = L_v \overline{v'W'} \qquad \mathcal{A} = -\frac{L_v \overline{W'^2}}{2}\left(\frac{\partial \overline{W}}{\partial y}\right)^{-1} \tag{36}$$

where we define $\mathcal{A}$ as the moisture mode activity. Here we note the similarity of $\mathcal{A}$ to Rossby wave activity (see Ch 10 in Vallis 2017). We include a negative sign in the definition of $\mathcal{A}$ so that it is a positive quantity, recalling that the mean meridional moisture gradient is equatorward (negative).

In order to obtain an equation that mirrors Eq. (36) but for the mean state, we integrate Eq. (35) meridionally from $-L_H$ to 0. Noting that there are no eddy moisture fluxes at the edges of the Hadley Cell, the resulting equation is written as:

$$\frac{\partial \mathrm{ALE}}{\partial t} = -L_v \overline{v'W'} \qquad \mathrm{ALE} = -\frac{L_H^2}{2}\frac{\partial L_v \overline{W}}{\partial y} \tag{37}$$

where we have defined a new variable, the "available latent energy" (ALE). Noting that the rhs of Eqs. (36) and (37) are equal and opposite, we can add them to obtain the following conservation relation:

$$\frac{\partial}{\partial t}(\mathrm{ALE} + \mathcal{A}) = 0. \tag{38}$$

We can now use Eq. (38) to define the ALE as the amount of latent energy that is available to be converted to moisture

mode activity $\mathcal{A}$. The magnitude of the ALE is directly proportional to the mean meridional moisture gradient. The relationship in Eq. (38) implies that moisture modes in this model grow by extracting ALE via MVI and hence flattening the mean moisture gradient.

On the contrary, a weakening of moisture mode activity implies a steepening of the mean meridional gradient. Because $[\overline{W}]$ has to remain constant in order to maintain RCE, it follows that the ALE also describes the strength of the Hadley Cell. When ALE is higher, the ITCZ is more humid and rainier while the subsiding branch is drier. Thus, the *moisture modes in this model grow at the expense of the Hadley Cell*.

This flattening effect can be seen more clearly if we invoke the flux-gradient hypothesis, i.e., $\overline{v'W'} = -\kappa_w \partial_y \overline{W}$. Using this approximation we can re-express Eq. (37) as:

$$\frac{\partial \mathrm{ALE}}{\partial t} = -\frac{\mathrm{ALE}}{\tau_D} \tag{39}$$

where $\tau_D = L_H^2/(2\kappa_w)$ is the ALE consumption timeacale. Scaling of the definition of κ_w suggests that it is roughly 3×10^{-5} m^2 s^{-1}, a value similar to that found by Neelin and Zeng (2000). Using this value we find that τ_D is roughly on the order of 20 days. Thus, while the consumption of ALE is slow compared to the timescale of the moisture modes, it is fast enough that it can have a significant impact at the intraseasonal timescale.

b. Lorenz energy cycle perspective of MVI

We can also interpret the exchange of energy between the mean state and the waves by invoking the Lorenz energy cycle (Lorenz 1955). Definitions of the acronyms and their respective budgets are shown in Appendix B. If we assume that the total energy of the system is in a steady state, we find that:

$$\frac{\partial}{\partial t}\left(\mathrm{APE}_Z + \mathrm{APE}_E + \mathrm{KE}_Z + \mathrm{KE}_E\right) = 0 \tag{40}$$

where APE and KE are the available potential energy and the kinetic energy, respectively. The subscript Z and E denote the zonal mean and eddy components of the energy, respectively.

Under the WTG approximation APE becomes much smaller than KE (see Appendix B), and the Lorenz energy cycle simplifies to a direct and proportional exchange between the zonal-mean KE and the eddy KE:

$$\frac{\partial \mathrm{KE}_Z}{\partial t} \simeq -\frac{\partial \mathrm{KE}_E}{\partial t}. \tag{41}$$

A schematic depiction of the simplified energy cycle is shown in Fig. 7b.

The similarity of Eq. (41) to Eq. (38) implies that they are related. We can show this relationship by combining Eqs. (14) - (16a) with Eq. (37)

$$\overline{u}_3 = -\frac{f_0}{S\epsilon\tau_c}\left(1 - \frac{y^2}{L_H^2}\right)\mathrm{ALE} \tag{42}$$

implying that

$$\frac{\partial}{\partial t}\left(\mathrm{KE}_Z, \mathrm{KE}_E\right) = \frac{8 f_0^2 \mathrm{ALE}}{15 S^2 \epsilon^2 \tau_c^2}\frac{\partial}{\partial t}\left(\mathrm{ALE}, \mathcal{A}\right) \tag{43}$$

where we have assumed that $\mathrm{KE}_Z \simeq \overline{u}_3^2/2$. Equation (43) shows that the KE of the Hadley Cell is proportional to ALE, while the circulation anomalies in the eddies are proportional to the moisture anomalies. This result suggests that the exchange of kinetic energy is related to how moisture is distributed by tropical circulations. Further, both tendencies are scaled by ALE, implying that KE conversions are stronger when the meridional moisture gradient is steeper. They are also stronger with larger f_0 due to the stronger vortex stretching that results, which increases KE. On the other hand, increasing S and τ_c would act to weaken vortex stretching because they weaken the P response to W anomalies. Lastly, increasing friction decreases KE through dissipation.

c. Steady state interactions under the presence of dissipation

Up to this point, we have only considered how moisture modes evolve when only linear interactions between the mean state and the waves are allowed. However, in part I we found that nonlinear horizontal moisture advection is a significant MSE sink, damping both equatorial Rossby waves and TD-like waves at all times. However, the damping is stronger in TD-like waves. Given that TD-like waves are smaller in scale than their Rossby wave counterparts, it is fair to assume that the nonlinear horizontal advection arises from mesoscale processes that act as a moisture diffusion, i.e. $\mathbf{v}' \cdot \boldsymbol{\nabla}_h W' \simeq -\kappa_W \nabla_h^2 W'$, where κ_W is a moisture diffusivity. For completeness, C' will also be included, even though its contribution is expected to be small. As a result, the modified equation for $\mathcal{A}$ is written as:

$$\frac{\partial \mathcal{A}}{\partial t} = \overline{v'W'} - \mathcal{D} \tag{44a}$$

$$\mathcal{D} = \frac{\kappa_W \overline{W'\nabla_h^2 W'}}{\partial_y \overline{W}} + \frac{\overline{C'W'}}{\partial_y \overline{W}} \tag{44b}$$

where $\mathcal{D}$ is defined as the dissipation of $\mathcal{A}$. If we no longer assume that Eq. (35) is satisfied for the zonal-mean state,

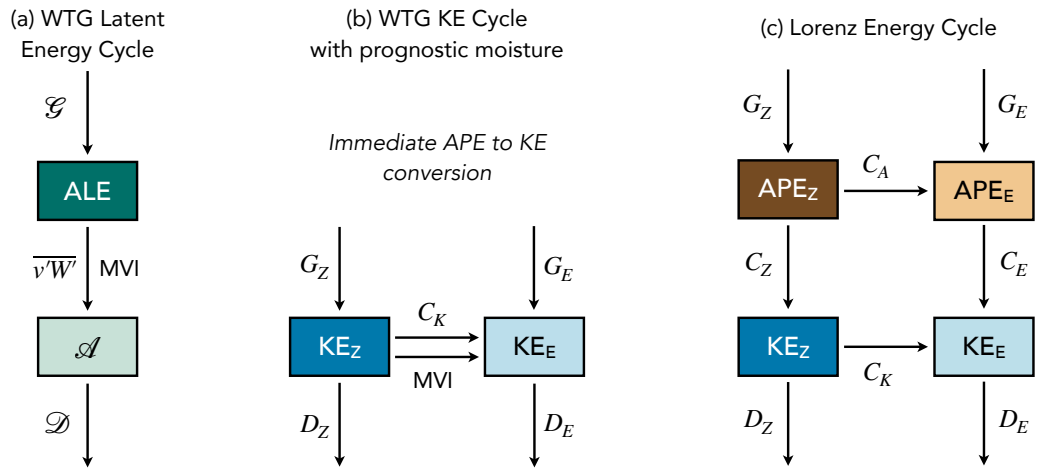

FIG. 7. Schematic showing the different energy cycles used in this study: (a) the WTG latent energy cycle, (b) the KE energy cycle under the WTG approximation, and (c) the conventional Lorenz energy cycle. See Appendix B for definitions of the terms in panels (b) and (c).

then the budget for ALE becomes

$$\frac{\partial \mathrm{ALE}}{\partial t} = -\overline{v'W'} + \mathcal{G} \tag{45}$$

where we have grouped the terms in Eq. (35) into a single ALE generation term:

$$\mathcal{G} = \frac{L_v}{L_H}\int_{-L_H}^{0} \overline{C}\,dy \tag{46}$$

where $\overline{C} = -\left(1 - \frac{L_v \overline{W}}{S}(1+r)\right)\frac{\overline{W}}{\tau_c} - \frac{\overline{W}}{S}R_{cs} + \overline{E}$ is the column process associated with the zonal-mean circulation.

In steady state, combining Eq. (45) with Eq. (44) leads to a balance between eddy dissipation and ALE generation:

$$\mathcal{D} = \mathcal{G}. \tag{47}$$

This result indicates that mean state motions act to amplify the Hadley Cell. However, the mean state is unstable and the added ALE is quickly consumed by eddies, which then dissipate. Thus, *latent energy follows a direct energy cascade, as in kinetic energy*.

Furthermore, if we assume that the horizontal scale of the eddies remains fixed, we find that $\mathcal{D} \sim 2\kappa_W K^2 \mathcal{A}$, so that Eq. (47) also indicates that wave activity is proportional to $\mathcal{G}$.

From the perspective of Eq. (44), the steady state can be used to obtain a diagnostic equation for the precipitation variance

$$\overline{P'^2} = -\frac{\overline{v'W'}}{\kappa_w K^2 \tau_c^2}\frac{\partial \overline{W}}{\partial y}. \tag{48}$$

This equation shows that precipitation variability along moisture gradients is stronger with a steeper gradient and with larger poleward eddy moisture fluxes, assuming that the other terms are fixed. Thus, while the ascending and descending branches of the Hadley Cell are steadily rainy and dry, respectively, the region in between is highly variable, fluctuating between rainy and dry periods associated with the passage of moisture modes.

From the perspective of the moisture budget, the balance of terms is written as

$$\frac{\partial \overline{v_3' W'}}{\partial y} = \overline{C} \tag{49}$$

implying that the column processes of the Hadley Cell moisten the atmosphere, while the eddy transport dries it. This result is consistent with the findings Inoue et al. (2021), who found that the column is unstable and that it is stabilized by horizontal moisture advection. We can show this by expanding the left-hand side of (49) using the chain rule,

$$\overline{v_3'\frac{\partial W'}{\partial y}} = \frac{L_v \overline{W'^2}}{S\tau_c}(1+r) + \overline{C} \tag{50}$$

where the first term on the rhs is the eddy column process. Since it is a positive quantity it adds to $\overline{C}$, and hence only the nonlinear horizontal moisture advection dries the troposphere.

Energy transports in the Hadley Cell are usually examined using the MSE budget. With the inclusion of eddies, the budget takes the following form

$$L_v \frac{\partial \overline{v_3' W'}}{\partial y} = -\frac{\partial \overline{v}_3 \overline{m}}{\partial y} + L_v \overline{E} + \langle \overline{Q}_r \rangle \tag{51}$$

where we are showing the eddy contribution on the left-hand side and the Hadley Cell component on the rhs. Since the eddies are in WTG balance, it follows that their con-

tribution to the MSE transport is governed by the latent energy component. As previously shown, $\overline{v_3'W'}$ must be poleward in order to balance the moisture diffusion, yielding a result that is consistent with the findings of Trenberth and Stepaniak (2003) and Rios-Berrios et al. (2020). Thus $\partial_y \overline{v_3'W'} > 0$ within the ITCZ, implying that the sum of the terms on the rhs of Eq. (51) must also be positive. Once again we find that the Hadley Cell would self-amplify in the absence of eddies.

d. Moisture modes as Hadley Cell predators

We will now generalize the results of this section and consider the case in which moisture mode-Hadley Cell interactions occur with both changes in time and dissipation. Let us begin by assuming that the results of the previous subsection correspond to the climatology, and that small deviations from this climatology exist. As a result, we can decompose the wave activity and the ALE into climatological (denoted by curly brackets) and fluctuating components:

$$\mathcal{A} = \{\mathcal{A}\} + \mathcal{A}^+ \tag{52a}$$

$$\text{ALE} = \{\text{ALE}\} + \text{ALE}^+. \tag{52b}$$

Let us consider the possibility that the moisture diffusivity κ_W is not a constant, but is instead proportional to $\mathcal{A}$. We reason this since $\overline{v}'W'$ is itself dependent on the strength of the moisture modes. Thus we write:

$$-\kappa_W \frac{\partial L_v \overline{W}}{\partial y} = \gamma \mathcal{A} \text{ALE} \tag{53}$$

where γ is a constant with units of mass per unit velocity with a rough value of 4×10^{-19} kg (m s)$^{-1}$, which we obtain from the Table 2 and the scales discussed in Section 3.

Now let us consider the climatology. As in Inoue and Back (2017), we assume that $\overline{C}$ is proportional to the ALE itself. By invoking Eq. (39) we find that $\mathcal{G} \sim \text{ALE}/\tau_D$. We can similarly assume that $\mathcal{D}$ is damping $\mathcal{A}$ via diffusion. Thus, it is reasonable to assume that $\mathcal{D} \sim -\mathcal{A}/\tau_D$. By making these approximations we find that the mean state balance is:

$$\{\mathcal{A}\} = \{\text{ALE}\} \qquad \gamma\{\text{ALE}\} = \tau_D^{-1} \tag{54}$$

Using Eqs. (52), (53), and (54) we can write Eqs. (44) and (45) as:

$$\frac{\partial \mathcal{A}^+}{\partial t} = \gamma\{\mathcal{A}\}\text{ALE}^+ \tag{55a}$$

$$\frac{\partial \text{ALE}^+}{\partial t} = -\gamma\{\text{ALE}\}\mathcal{A}^+. \tag{55b}$$

Equation (55) is a linear predator-prey system (Majda and Stechmann 2009), with the moisture modes behaving as the predator and the Hadley Cell being the prey. The solution to this system is an oscillation with a frequency:

$$\varpi = \pm\gamma\{\text{ALE}\} \tag{56}$$

That is, the coupled system exhibits an oscillation. A quick inspection of the definition of ALE suggests that it has a mean value of 10^{13} J m^{-1}. With the estimated value of γ we find that the oscillation has a timescale of ~35 days. Given that this value was obtained from an estimation with a high amount of uncertainty, it is possible that this value could vary by a factor of 2. Nonetheless, the oscillation would still occur at the intraseasonal timescale.

To qualitatively understand the nature of this predator-prey system, it is useful to invoke the chain rule $\frac{\partial \text{ALE}^+}{\partial t} = \frac{\partial \text{ALE}^+}{\partial \mathcal{A}^+}\frac{\partial \mathcal{A}^+}{\partial t}$, from which we obtain the following equality:

$$\text{ALE}^{+2} + \mathcal{A}^{+2} = \text{constant}. \tag{57}$$

This result implies that there is a circular cycle in the ALE-$\mathcal{A}$ phase space. This cycle, shown in Fig. 8, implies that periods of high ALE are followed by periods of high wave activity. Since the wave activity reduces the ALE, the reverse part of the cycle ensues.

5. Discussion and Conclusions

In recent decades our understanding of tropical atmospheric motions has grown expeditiously (Emanuel 2018; Jiang et al. 2020; Adames and Maloney 2021). Part of this growth has been due to the increased awareness of the importance of water vapor in these motions (Inoue and Back 2017; Wolding et al. 2020; Maithel and Back 2022). As our understanding continues improving we have recognized that "moisture modes" may exist in the tropics. Initially used to describe the MJO (Raymond and Fuchs 2009; Sobel and Maloney 2013), recent studies have posited that moisture modes may be a more common feature of the tropics (Adames and Maloney 2021; Inoue et al. 2021; Maithel and Back 2022; Adames 2022). There is increasing evidence that convectively-coupled equatorial Rossby waves and tropical depression-like waves may be moisture modes as well (Inoue et al. 2020; Gonzalez and Jiang 2019; Nakamura and Takayabu 2022a; Mayta et al. 2022). In part I we showed that these moisture modes share similar MSE budgets; zonal MSE advection governs their propagation while meridional MSE plays a central role in their growth.

On the basis of these findings, we investigated the possibility that moisture modes interact with the Hadley Cell. To do this, we employed the two-layer model of Adames et al. (2021) and adapted it to accommodate an idealized Hadley Cell. The strength of the Hadley Cell is assumed to be proportional to the mean meridional moisture gradient. The overturning circulation is found to be in WTG balance so long as the square of its meridional half-width (L_H^2) is

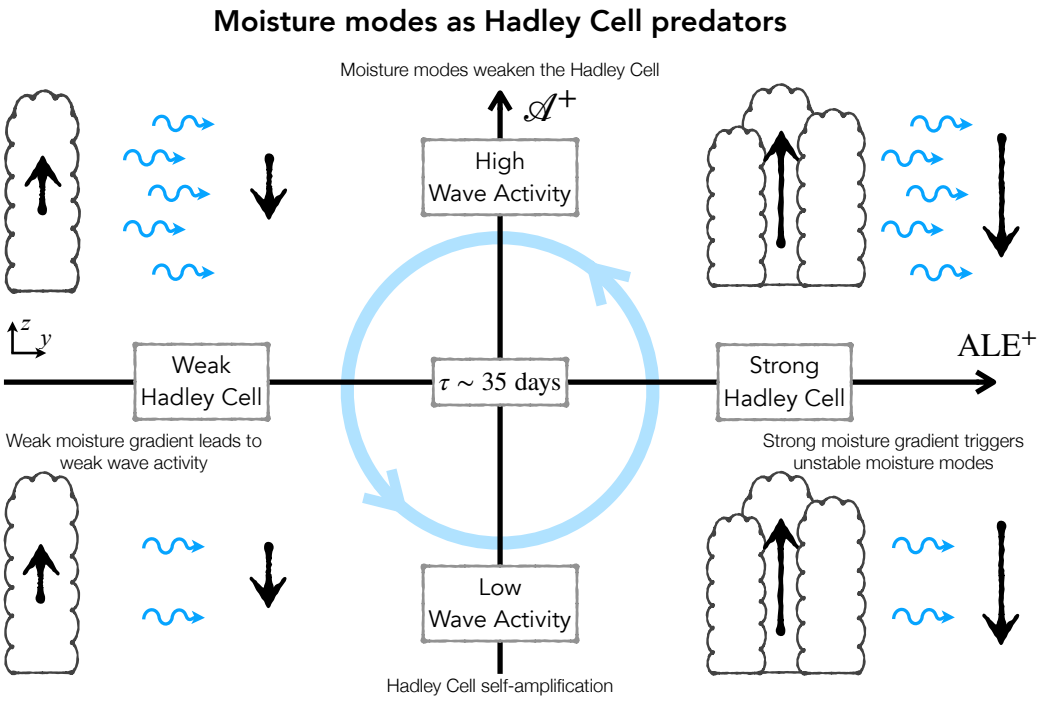

FIG. 8. Schematic describing the predator-prey relationship between moisture modes and the Hadley Cell according to the results of Section 4d. The x- and y-axis show ALE and wave activity ($\mathcal{A}$) deviations from climatology. The drawings in each quadrant depict the strength of the Hadley Cell (clouds) and the amount of wave activity (wavy arrows).

smaller than the square of the Rossby radius of deformation (L_d^2).

If the mean state is simplified further by assuming the mean lower-tropospheric winds are constant, we obtain a system of equations that are nearly identical to those of Sobel et al. (2001), but with a restricted meridional scale. Wave solutions to this idealized mean state yield a pair of wave solutions, one of which is unstable. The unstable solution propagates westward from a combination of zonal advection by the mean flow and meridional advection of the mean moisture by the anomalous meridional winds. It is destabilized by the latter process. The most unstable wave grows near zonal wavenumber 10 and propagates westward at roughly the same speed as the trade winds. The contributions of horizontal moisture advection to propagation and growth are consistent with the TD-like waves documented in part I, which also exhibit their strongest growth near zonal wavenumber 10.

An interesting result of Eq. (33) is that the ± sign before the term on the square root implies that one of the wave solutions will always be unstable, so long as the square root is nonzero. For example, a growing solution still exists if the moisture gradient is poleward, as we observe in the south Asian monsoon (Clark et al. 2020). This result means that a meridional moisture gradient in the presence of rotation (nonzero f) will always be unstable so long as convection is sensitive to water vapor fluctuations.

We then return to the original Hadley Cell model to examine if transients that grow from meridional moisture advection interact with the Hadley Cell. Our results show that moisture mode activity increases when there are poleward moisture fluxes. The pair of equations that describe the interaction between moisture modes and the Hadley Cell (Eqs. 36 and 37) are analogous to the Eliasen-Palm flux formulation (Andrews and Mcintyre 1976; Edmon Jr et al. 1980), with column water vapor taking the place of potential vorticity.

Examination of this pair of equations reveals that the eddy moisture fluxes flatten the mean meridional moisture gradient, therefore weakening the Hadley Cell, as summarized in Fig. 9. Thus, a stronger ITCZ is associated with drier subtropics, consistent with previous work (Hohenegger and Jakob 2020; Popp et al. 2020). Furthermore, we found that the amplification of moisture modes at the expense of the Hadley Cell is transient, as the available latent energy (ALE) for moisture mode activity decreases with a weakening Hadley Cell. Such a transient behavior leads to a cycle, where moisture modes deplete the ALE and hence weaken the Hadley Cell, followed by a period of weak moisture mode activity where the Hadley Cell and the ALE rebuild. This oscillation occurs at the subseasonal timescale, and it is not clear if it may be associated with the MJO. Nonetheless, this result may provide

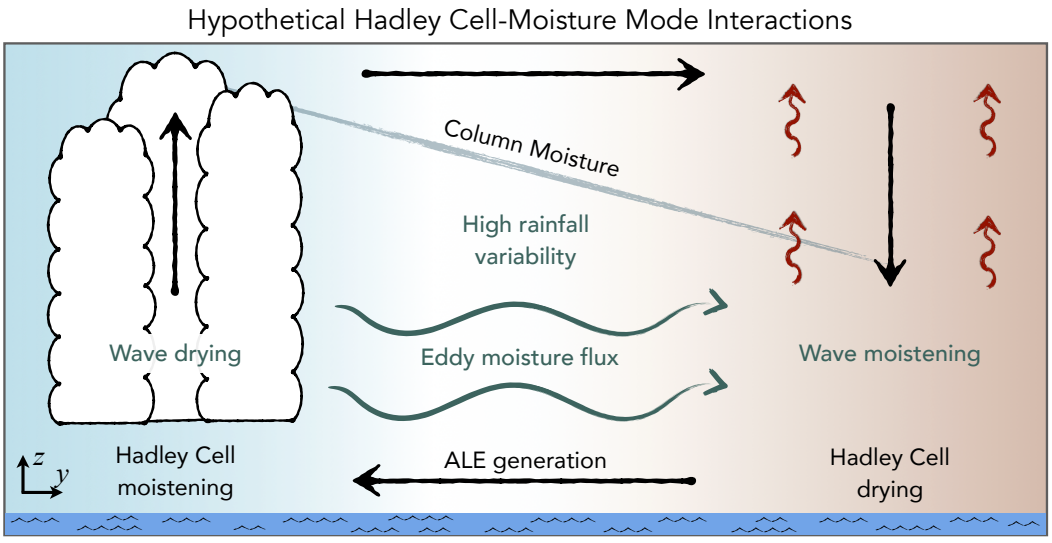

FIG. 9. As in Fig 2 but showing how moisture modes interact with the Hadley Cell according to the results of this study. The green wavy lines depict the eddy moisture flux and the light line above it shows the mean W distribution.

useful directions for improving prediction at the seasonal-to-subseasonal timescale.

That the latent energy fluxes are poleward also suggests that they may be important for global energy transport. Eddy energy fluxes in the tropics are smaller than those in the midlatitudes, but they are not negligible (Fig. 1 in Trenberth and Stepaniak (2003) and Fig. 5 in Rios-Berrios et al. (2020)). These eddy fluxes are dominated by the latent energy component, with DSE transports being negligible, as would be expected from moisture modes.

An interesting interpretation of the results of this study comes from examining them from the perspective of convective self-aggregation (Bretherton et al. 2005; Wing and Emanuel 2014; Windmiller and Craig 2019). We can interpret the tendency of the Hadley Cell to amplify through column processes as a tendency for the ITCZ to aggregate through radiative-convective instability (Emanuel et al. 2014). In this case, the MSE/moisture variance in the ITCZ will increase, consistent with an increase in ALE. Under this lens, moisture mode activity would act to disaggregate the ITCZ by diffusing the moisture distribution. Examining the results of this study from the view of aggregation could be a fruitful direction for future research.

From the perspective of the Lorenz (1955) energy cycle, we found that the WTG approximation reduces the energy cycle to solely be about kinetic energy conversions. Within this context, moisture modes tap into the kinetic energy of the Hadley Cell – the trade winds being the main reservoir – and convert it into eddy kinetic energy. This conversion is another consequence of the flattening of the moisture gradient.

Extending these results to zonal moisture gradients can yield some interesting insights into the nature of Rossby waves and the MJO. Since the MJO is strongest over the Indian Ocean, a region characterized by an eastward and equatorward moisture gradient, it is possible that the MJO is diffusing latent energy from the Maritime Continent. Hence, the MJO moistens the Indian Ocean at the expense of moisture over the Maritime Continent. Some western Pacific equatorial Rossby waves may work analogously. Thus, both these systems would gain energy while weakening the Walker Cell.

We recognize that the results of this study were obtained using an idealized two-layer model with numerous assumptions and approximations. First, the two-layer model only accounts for the first baroclinic vertical motions. Second baroclinic motions can be important, especially in determining the net stability of the column (Inoue et al. 2020). Second, by assuming the motions exist within a Hadley Cell bounded by rigid lids we are neglecting the role the extratropics may have in determining the mean state in which the wave propagates. We are also ignoring the beta effect and any contribution that temperature fluctuations have to precipitation variability. More work is needed to understand whether the results of this study are still valid in a more realistic setting.

We conclude this study by returning to the first paragraph of Section 1. In spite of the acknowledgment that the tropics exhibit a diversity of motion systems, there is a lack of work done trying to understand how these systems interact with the mean circulation. Most studies assume the Hadley Cell to be a stable circulation and the most important source of energy transport out of the tropics. This study challenges this notion. Results from part I and other previous works (Inoue et al. 2021; Maithel and Back 2022) suggest that horizontal moisture advection may be impor-

tant in understanding rainfall variability and the growth of large-scale waves. Results from this work agree with these studies and reveal that horizontal moisture advection plays a central role in interactions between the Hadley Cell and the waves. These interactions are analogous to those of baroclinic eddies and the jet stream. While baroclinic instability weakens the jet stream by flattening the temperature gradient, moisture modes weaken the Hadley Cell by flattening the moisture gradient. These interactions are mediated by a poleward eddy moisture flux, which may play an important role in the global energy balance. If these results are confirmed by future studies, they would imply that the tropical atmosphere is even richer and more dynamic than previously thought, implying that the words written in the prologue of Riehl (1954) still resonate today.

Acknowledgments. ÁFAC was supported by NSF CAREER grant number 2236433, and by the University of Wisconsin startup package. VM was supported by NOAA grant number NA22OAR4310611. ÁFAC would like to thank his late father, Ángel David Adames Tomassini, for listening to and motivating him to complete this project in spite of strenuous circumstances. The contents of the manuscript were significantly improved after conversations with Rosimar Ríos Berríos and Rich Rotunno. Conversations with Kerry Emanuel also helped improve the interpretation of the results of this study. Discussions with J. M. Wallace helped understand the Lorenz energy cycle under WTG balance. We thank Haochang Luo for reviewing an early version of this manuscript.

Data availability statement. ERA5 data is available at: https://www.ecmwf.int/en/forecasts/datasets/reanalysis-datasets/era5/). Interpolated T_b data are provided by the NOAA/ESRL.

APPENDIX A

Comparison between evaporation and advection

The bulk aerodynamic formula for surface evaporation is written as:

$$E = C_q \rho_4 |\mathbf{v}_4| q_4^* (1 - \mathrm{RH}_4) \tag{A1}$$

where $C_q \simeq 10^{-3}$ is a bulk exchange coefficient, q_4^* is the saturation specific humidity near the surface (layer 4), and $\mathrm{RH}_4 = q_4/q_4^*$ is the surface relative humidity. The wind speed has a contribution from the mean flow and the eddies. If we assume that the zonal wind is predominantly determined by the mean trade winds, while the meridional winds come from the eddies, then we can approximate the total wind speed as:

$$|\mathbf{v}_4| = \sqrt{u_4^2 + v_4^2} \simeq \sqrt{\overline{u}_4^2 + v_4'^2}. \tag{A2}$$

If we assume that $\overline{u}^2 \gg v'^2$, we can perform a Taylor series expansion on $|\mathbf{v}|$, yielding:

$$|\mathbf{v}_4| \simeq |\overline{u}_4| + \frac{v_4'^2}{2|\overline{u}_4|}. \tag{A3}$$

When decomposing $E = \overline{E} + E'$, we obtain:

$$E' = \frac{v_4'^2}{2|\overline{u}_4|} C_q \rho_4 q_4^* (1 - \mathrm{RH}_4). \tag{A4}$$

Using realistic surface values $\rho \sim 1$ kg m^{-3}, $q_4^* \sim 0.02$, 1-RH$_4 \sim 0.2$, $v_4' \sim 1$ m s^{-1} and $\overline{u}_4 \sim 4$ m s^{-1} we obtain that $L_v E' \sim 1$ W m^{-2}. Thus, the evaporation anomalies are much weaker than the anomalies in horizontal moisture advection.

APPENDIX B

Kinetic energy cycle under WTG balance

The budgets for eddy APE and KE are written following Lorenz (1955); Norquist et al. (1977); Hsieh and Cook (2007), and Rydbeck and Maloney (2014):

$$\frac{\partial \mathrm{APE}_Z}{\partial t} = -C_A - C_Z + G_Z \tag{B1a}$$

$$\frac{\partial \mathrm{APE}_E}{\partial t} = C_A - C_E + G_E \tag{B1b}$$

$$\frac{\partial \mathrm{KE}_E}{\partial t} = C_E + C_K - D_E \tag{B1c}$$

$$\frac{\partial \mathrm{KE}_Z}{\partial t} = C_Z - C_K - D_Z \tag{B1d}$$

where APE and KE are the available potential energy and the kinetic energy, with the subscript Z and E denoting the zonal mean component and the eddy component, respectively. Their definitions are as follows:

$$\mathrm{APE}_Z = \left\langle \frac{C_p \gamma [\overline{T}^{*2}]}{2[\overline{T}]} \right\rangle \quad \mathrm{APE}_E = \left\langle \frac{C_p \gamma [\overline{T'^2}]}{2[\overline{T}]} \right\rangle \tag{B2a}$$

$$\mathrm{KE}_Z = \left\langle \frac{[\overline{u}^2 + \overline{v}^2]}{2} \right\rangle \quad \mathrm{KE}_E = \left\langle \frac{[\overline{u'^2 + v'^2}]}{2} \right\rangle \tag{B2b}$$

where asterisks denote departures from the meridional mean, i.e.:

$$\overline{T}^* = \overline{T} - [\overline{T}] \tag{B3}$$

and

$$\gamma = -\frac{R_d [\overline{T}]}{p \partial_p s} = \frac{\partial_p [\overline{\Phi}]}{\partial_p s}. \tag{B4}$$

The terms on the rhs of Eq. (B1) are the conversion of APE_Z to APE_E:

$$C_A = -\left\langle \left[C_p \gamma \frac{\overline{v'T'}}{[\overline{T}]} \frac{\partial \overline{T}}{\partial y} \right] \right\rangle - \left\langle \left[C_p \gamma \frac{\overline{\omega'T'}}{[\overline{T}]} \frac{\partial \overline{T}^*}{\partial p} \right] \right\rangle, \quad \text{(B5a)}$$

the conversion of KE_Z to KE_E (i.e. the barotropic energy conversion)

$$C_K \simeq -\left\langle \left[\overline{u'v'} \frac{\partial \overline{u}}{\partial y} \right] \right\rangle - \left\langle \left[\overline{v'^2} \frac{\partial \overline{v}}{\partial y} \right] \right\rangle, \quad \text{(B5b)}$$

the conversion of APE to KE (i.e. the baroclinic energy conversion):

$$C_Z = \left\langle \frac{R_d [\overline{\omega}^* \overline{T}^*]}{p} \right\rangle \qquad C_E = \left\langle \frac{R_d [\overline{\omega'T'}]}{p} \right\rangle, \quad \text{(B5c)}$$

the kinetic energy dissipation

$$D_Z = 2\epsilon K_Z \qquad D_E = 2\epsilon K_E \quad \text{(B5d)}$$

and the generation of APE

$$G_Z = \left\langle \frac{[\gamma \overline{T}^* \overline{Q}^*]}{[\overline{T}]} \right\rangle \qquad G_E = \left\langle \frac{[\gamma \overline{T'Q'}]}{[\overline{T}]} \right\rangle \quad \text{(B5e)}$$

Under WTG balance, the scaling of the thermodynamic equation translates to the APE budget. That is, C_A and the tendency in APE are much smaller than G_E and the baroclinic energy conversion C_E. Thus, the leading order balance in the APE budget is:

$$C_Z \simeq G_Z \quad \text{(B6a)}$$

$$C_E \simeq G_E \quad \text{(B6b)}$$

a result that was found by Rydbeck and Maloney (2014) in east Pacific easterly waves. It is important to note that the terms contain T' and $\overline{T}^*$, indicating that temperature fluctuations in space and time are important in circulations that satisfy WTG balance, even though they are small.

The result shown in Eq. (B6) indicates that baroclinic energy conversions quickly convert APE to KE. As a result, G_E is effectively a generator of KE under WTG balance. We can show this by inserting Eq. (B6) into the KE_E budget to obtain:

$$\frac{\partial \mathrm{KE}_Z}{\partial t} = G_Z - C_K - D_Z \quad \text{(B7a)}$$

$$\frac{\partial \mathrm{KE}_E}{\partial t} = G_E + C_K - D_E. \quad \text{(B7b)}$$

If the circulation is in a steady state then the total kinetic energy in the system is fixed, and hence the sources and sinks of KE_Z and KE_E must cancel one another:

$$G_E + G_Z = D_Z + D_E \quad \text{(B8)}$$

and the budgets in (B7) can be added to obtain Eq. (41).

References

Adames, Á. F., 2021: Interactions between water vapor, potential vorticity and vertical wind shear in quasi-geostrophic motions: Implications for rotational tropical motion systems. *Journal of the Atmospheric Sciences*, https://doi.org/10.1175/JAS-D-20-0205.1.

Adames, Á. F., 2022: The basic equations underweak temperature gradient balance: Formulation, scaling, and types of convectively-coupled motions. *Journal of the Atmospheric Sciences*.

Adames, Á. F., D. Kim, S. K. Clark, Y. Ming, and K. Inoue, 2019: Scale Analysis of Moist Thermodynamics in a Simple Model and the Relationship between Moisture Modes and Gravity Waves. *Journal of the Atmospheric Sciences*, **76 (12)**, 3863–3881, https://doi.org/10.1175/JAS-D-19-0121.1.

Adames, Á. F., D. Kim, A. H. Sobel, A. Del Genio, and J. Wu, 2017: Characterization of moist processes associated with changes in the propagation of the mjo with increasing co2. *Journal of Advances in Modeling Earth Systems*, **9 (8)**, 2946–2967, https://doi.org/10.1002/2017MS001040.

Adames, Á. F., and E. D. Maloney, 2021: Moisture Mode Theory's Contribution to Advances in our Understanding of the Madden-Julian Oscillation and Other Tropical Disturbances. *Current Climate Change Reports*, https://doi.org/10.1007/s40641-021-00172-4.

Adames, Á. F., R. M. V. Martes, H. Luo, and R. B. Rood, 2022: Moist static potential vorticity budget in tropical motion systems. *Journal of the Atmospheric Sciences*, **79 (3)**, 763–779.

Adames, A. F., and Y. Ming, 2018: Interactions between Water Vapor and Potential Vorticity in Synoptic-Scale Monsoonal Disturbances: Moisture Vortex Instability. *Journal of the Atmospheric Sciences*, **75 (6)**, 2083–2106, https://doi.org/10.1175/JAS-D-17-0310.1.

Adames, Á. F., S. W. Powell, F. Ahmed, V. C. Mayta, and J. D. Neelin, 2021: Tropical precipitation evolution in a buoyancy-budget framework. *Journal of the Atmospheric Sciences*, **78 (2)**, 509 – 528, https://doi.org/10.1175/JAS-D-20-0074.1.

Ahmed, F., Á. F. Adames, and J. D. Neelin, 2020: Deep Convective Adjustment of Temperature and Moisture. *Journal of the Atmospheric Sciences*, **77 (6)**, 2163–2186, https://doi.org/10.1175/JAS-D-19-0227.1.

Ahmed, F., and J. D. Neelin, 2018: Reverse engineering the tropical precipitation–buoyancy relationship. *J. Atmos. Sci.*, **75 (5)**, 1587–1608, https://doi.org/10.1175/JAS-D-17-0333.1.

Andersen, J. A., and Z. Kuang, 2012: Moist Static Energy Budget of MJO-like Disturbances in the Atmosphere of a Zonally Symmetric Aquaplanet. *J. Climate*, **25 (8)**, 2782–2804.

Andrews, D., and M. E. Mcintyre, 1976: Planetary waves in horizontal and vertical shear: The generalized eliassen-palm relation and the mean zonal acceleration. *Journal of Atmospheric Sciences*, **33 (11)**, 2031–2048.

Bretherton, C. S., P. N. Blossey, and M. Khairoutdinov, 2005: An energy-balance analysis of deep convective self-aggregation above uniform SST. *J. Atmos. Sci.*, **62 (12)**, 4273–4292.

Bretherton, C. S., M. E. Peters, and L. E. Back, 2004: Relationships between Water Vapor Path and Precipitation over the Tropical Oceans. *J. Climate*, **17**, 1517–1528.

Bretherton, C. S., and P. K. Smolarkiewicz, 1989: Gravity Waves, Compensating Subsidence and Detrainment around Cumulus Clouds. *J. Atmos. Sci.*, **46 (6)**, 740–759, https://doi.org/10.1175/1520-0469(1989)046⟨0740:GWCSAD⟩2.0.CO;2.

Chang, C.-P., 1970: Westward propagating cloud patterns in the tropical pacific as seen from time-composite satellite photographs. *J. Atmos. Sci.*, **27 (1)**, 133–138, https://doi.org/10.1175/1520-0469(1970)027⟨0133:WPCPIT⟩2.0.CO;2.

Charney, J. G., 1963: A Note on Large-Scale Motions in the Tropics. *J. Atmos. Sci.*, **20 (6)**, 607–609.

Chen, G., 2022a: The amplification of madden–julian oscillation boosted by temperature feedback. *Journal of the Atmospheric Sciences*, **79 (1)**, 51–72.

Chen, G., 2022b: A model of the convectively coupled equatorial rossby wave over the indo-pacific warm pool. *Journal of the Atmospheric Sciences*, **79 (9)**, 2267–2283.

Chikira, M., 2014: Eastward-propagating intraseasonal oscillation represented by Chikira–Sugiyama cumulus parameterization. Part II: Understanding moisture variation under weak temperature gradient balance. *J. Atmos. Sci.*, **71 (2)**, 615–639.

Ciesielski, P. E., R. H. Johnson, P. T. Haertel, and J. Wang, 2003: Corrected toga coare sounding humidity data: Impact on diagnosed properties of convection and climate over the warm pool. *Journal of climate*, **16 (14)**, 2370–2384.

Clark, S. K., Y. Ming, and Á. F. Adames, 2020: Monsoon low pressure system–like variability in an idealized moist model. *Journal of Climate*, **33 (6)**, 2051–2074.

de Szoeke, S. P., 2018: Variations of the moist static energy budget of the tropical indian ocean atmospheric boundary layer. *Journal of the Atmospheric Sciences*, **75 (5)**, 1545–1551, https://doi.org/10.1175/JAS-D-17-0345.1.

Edmon Jr, H., B. Hoskins, and M. McIntyre, 1980: Eliassen-palm cross sections for the troposphere. *Journal of Atmospheric Sciences*, **37 (12)**, 2600–2616.

Emanuel, K., 2018: 100 years of progress in tropical cyclone research. *Meteorological Monographs*, **59**, 15–1.

Emanuel, K., 2019: Inferences from simple models of slow, convectively coupled processes. *Journal of the Atmospheric Sciences*, **76 (1)**, 195–208, https://doi.org/10.1175/JAS-D-18-0090.1.

Emanuel, K., A. A. Wing, and E. M. Vincent, 2014: Radiative-convective instability. *J. Adv. Model. Earth Syst.*, **6 (1)**, 75–90.

Gonzalez, A. O., and X. Jiang, 2019: Distinct propagation characteristics of intraseasonal variability over the tropical west pacific. *Journal of Geophysical Research: Atmospheres*, **124 (10)**, 5332–5351, https://doi.org/10.1029/2018JD029884.

Hartmann, D. L., 2015: *Global physical climatology*, Vol. 103. Newnes.

Herman, M. J., Ž. Fuchs, D. J. Raymond, and P. Bechtold, 2016: Convectively coupled kelvin waves: From linear theory to global models. *J. Atmos. Sci.*, **73 (1)**, 407–428, https://doi.org/10.1175/JAS-D-15-0153.1.

Hohenegger, C., and C. Jakob, 2020: A relationship between itcz organization and subtropical humidity. *Geophysical Research Letters*, **47 (16)**, e2020GL088 515, https://doi.org/https://doi.org/10.1029/2020GL088515.

Holton, J. R., and G. J. Hakim, 2012: *An Introduction to Dynamic Meteorology*. Academic Press.

Hsieh, J.-S., and K. H. Cook, 2007: A Study of the Energetics of African Easterly Waves Using a Regional Climate Model. *J. Atmos Sci.*, **64**, 421–440, https://doi.org/10.1175/JAS3851.1.

Inoue, K., Á. F. Adames, and K. Yasunaga, 2020: Vertical Velocity Profiles in Convectively Coupled Equatorial Waves and MJO: New Diagnoses of Vertical Velocity Profiles in the Wavenumber–Frequency Domain. *Journal of the Atmospheric Sciences*, **77 (6)**, 2139–2162, https://doi.org/10.1175/JAS-D-19-0209.1.

Inoue, K., and L. E. Back, 2017: Gross moist stability analysis: Assessment of satellite-based products in the gms plane. *J. Atmos. Sci.*, **74 (6)**, 1819–1837, https://doi.org/10.1175/JAS-D-16-0218.1.

Inoue, K., M. Biasutti, and A. M. Fridlind, 2021: Evidence that horizontal moisture advection regulates the ubiquitous amplification of rainfall variability over tropical oceans. *Journal of the Atmospheric Sciences*, **78 (2)**, 529 – 547, https://doi.org/10.1175/JAS-D-20-0201.1.

Jensen, M. P., and A. D. Del Genio, 2006: Factors limiting convective cloud-top height at the arm nauru island climate research facility. *Journal of climate*, **19 (10)**, 2105–2117.

Jiang, X., and Coauthors, 2020: Fifty years of research on the madden-julian oscillation: Recent progress, challenges, and perspectives. *Journal of Geophysical Research: Atmospheres*, **125 (17)**, e2019JD030 911, https://doi.org/10.1029/2019JD030911.

Kerns, B. W., and S. S. Chen, 2014: Equatorial dry air intrusion and related synoptic variability in mjo initiation during dynamo. *Monthly Weather Review*, **142 (3)**, 1326–1343.

Kiladis, G. N., M. C. Wheeler, P. T. Haertel, K. H. Straub, and P. E. Roundy, 2009: Convectively Coupled Equatorial Waves. *Rev. Geophys.*, 1–42.

Kim, D., M.-S. Ahn, I.-S. Kang, and A. D. Del Genio, 2015: Role of Longwave Cloud–Radiation Feedback in the Simulation of the Madden–Julian Oscillation. *J. Climate*, **28**, 6979–6994.

Lorenz, E. N., 1955: Available potential energy and the maintenance of the general circulation. *Tellus*, **7 (2)**, 157–167.

Madden, R., and P. Julian, 1972: Further Evidence of Global-Scale 5-Day Pressure Waves. *J. Atmos. Sci.*, **29 (8)**, 1464–1469.

Maithel, V., and L. Back, 2022: Moisture recharge–discharge cycles: A gross moist stability–based phase angle perspective. *Journal of the Atmospheric Sciences*, **79 (9)**, 2401–2417.

Majda, A. J., and S. N. Stechmann, 2009: The skeleton of tropical intraseasonal oscillations. *Proc. Natl. Acad. Sci. USA*, **106 (21)**, 8417–8422, https://doi.org/10.1073/pnas.0903367106.

Manabe, S., and R. F. Strickler, 1964: Thermal equilibrium of the atmosphere with a convective adjustment. *J. Atmos. Sci.*, **21 (4)**, 361–385.

Mapes, B. E., and P. Zuidema, 1996: Radiative-dynamical consequences of dry tongues in the tropical troposphere. *Journal of Atmospheric Sciences*, **53 (4)**, 620–638.

Matsuno, T., 1966: Quasi-geostrophic motions in the equatorial area. *J. Meteor. Soc. Japan*, **44**, 25–43.

Mayta, V. C., and Á. F. Adames, 2023: Moist Thermodynamics of Convectively Coupled Waves over the Western Hemisphere. *Journal of Climate*, 1–35, https://doi.org/10.1175/JCLI-D-22-0435.1.

Mayta, V. C., Á. F. Adames, and F. Ahmed, 2022: Westward-propagating moisture mode over the tropical western hemisphere. *Geophysical Research Letters*, e2022GL097799.

Mayta, V. C., and Á. F. Adames-Corraliza, 2023: Is the Madden-Julian Oscillation a Moisture Mode? *Authorea Preprints*.

Mayta, V. C., and Á. F. Adames Corraliza, 2023: The Stirring Tropics. Part I: The Ubiquity of Moisture Modes and Moisture-Vortex Instability. *Journal of Climate*.

Mooley, D. A., 1973: Some aspects of indian monsoon depressions and the associated rainfall. *Monthly Weather Review*, **101 (3)**, 271–280.

Nakamura, Y., and Y. N. Takayabu, 2022a: Convective couplings with equatorial rossby waves and equatorial kelvin waves. part i: Coupled wave structures. *Journal of the Atmospheric Sciences*, **79 (1)**, 247–262.

Nakamura, Y., and Y. N. Takayabu, 2022b: Convective couplings with equatorial rossby waves and equatorial kelvin waves. part ii: Coupled precipitation characteristics. *Journal of the Atmospheric Sciences*, **79 (11)**, 2919–2933.

Neelin, J. D., and I. M. Held, 1987: Modeling Tropical Convergence Based on the Moist Static Energy Budget. *Mon. Wea. Rev.*, **115**, 3–12.

Neelin, J. D., and N. Zeng, 2000: A Quasi-Equilibrium Tropical Circulation Model—Formulation*. *J. Atmos. Sci.*, **57 (11)**, 1741–1766.

Norquist, D. C., E. E. Recker, and R. J. Reed, 1977: The energetics of african wave disturbances as observed during phase iii of gate. *Monthly Weather Review*, **105 (3)**, 334–342.

Núñez Ocasio, K. M., and R. Rios-Berrios, 2023: African Easterly Wave Evolution and Tropical Cyclogenesis in a Pre-Helene (2006) Hindcast Using the Model for Prediction Across Scales-Atmosphere (MPAS-A). *Journal of Advances in Modeling Earth Systems*, **15 (2)**, e2022MS003 181, https://doi.org/https://doi.org/10.1029/2022MS003181.

Parsons, D. B., J.-L. Redelsperger, and K. Yoneyama, 2000: The evolution of the tropical western pacific atmosphere-ocean system following the arrival of a dry intrusion. *Quarterly Journal of the Royal Meteorological Society*, **126 (563)**, 517–548.

Peters, M. E., and C. S. Bretherton, 2005: A simplified model of the Walker circulation with an interactive ocean mixed layer and cloud-radiative feedbacks. *J. Climate*, **18 (20)**, 4216–4234.

Pierrehumbert, R., 1998: Lateral mixing as a source of subtropical water vapor. *Geophysical research letters*, **25 (2)**, 151–154.

Popp, M., N. J. Lutsko, and S. Bony, 2020: The relationship between convective clustering and mean tropical climate in aquaplanet simulations. *Journal of advances in modeling earth systems*, **12 (8)**, e2020MS002 070.

Powell, S. W., 2017: Successive mjo propagation in merra-2 reanalysis. *Geophysical Research Letters*, **44 (10)**, 5178–5186, https://doi.org/10.1002/2017GL073399.

Raymond, D. J., and Ž. Fuchs, 2009: Moisture Modes and the Madden–Julian Oscillation. *J. Climate*, **22**, 3031–3046.

Raymond, D. J., S. L. Sessions, and Ž. Fuchs, 2007: A theory for the spinup of tropical depressions. *Quart. J. Roy. Meteor. Soc.*, **133 (628)**, 1743–1754, https://doi.org/10.1002/qj.125.

Riehl, H., 1954: Tropical meteorology. Tech. rep., McGraw-hill.

Rios-Berrios, R., F. Judt, G. Bryan, B. Medeiros, and W. Wang, 2023: Three-Dimensional Structure of Convectively Coupled Equatorial Waves in Aquaplanet Experiments with Resolved or Parameterized Convection. *Journal of Climate*, 1 – 44, https://doi.org/10.1175/JCLI-D-22-0422.1.

Rios-Berrios, R., B. Medeiros, and G. Bryan, 2020: Mean climate and tropical rainfall variability in aquaplanet simulations using the model for prediction across scales-atmosphere. *Journal of Advances in Modeling Earth Systems*, **12 (10)**, e2020MS002 102.

Rushley, S. S., D. Kim, C. S. Bretherton, and M.-S. Ahn, 2018: Reexamining the Nonlinear Moisture-Precipitation Relationship Over the Tropical Oceans. *Geophys. Res. Lett.*, https://doi.org/10.1002/2017GL076296.

Rydbeck, A. V., and E. D. Maloney, 2014: Energetics of east pacific easterly waves during intraseasonal events. *Journal of Climate*, **27 (20)**, 7603–7621.

Serra, Y. L., G. N. Kiladis, and M. F. Cronin, 2008: Horizontal and Vertical Structure of Easterly Waves in the Pacific ITCZ. *J. Atmos. Sci.*, **65**, 1266–1284, https://doi.org/10.1175/2007JAS2341.1.

Sherwood, S. C., 1996: Maintenance of the free-tropospheric tropical water vapor distribution. part i: Clear regime budget. *Journal of climate*, **9 (11)**, 2903–2918.

Sobel, A., and E. Maloney, 2013: Moisture Modes and the Eastward Propagation of the MJO. *J. Atmos. Sci.*, **70**, 187–192.

Sobel, A., S. Wang, and D. Kim, 2014: Moist static energy budget of the MJO during DYNAMO. *J. Atmos. Sci.*, **71**, 4276–4291.

Sobel, A. H., and C. S. Bretherton, 2000: Modeling Tropical Precipitation in a Single Column. *J. Climate*, **13**, 4378–4392.

Sobel, A. H., J. Nilsson, and L. M. Polvani, 2001: The Weak Temperature Gradient Approximation and Balanced Tropical Moisture Waves. *J. Atmos. Sci.*, **58**, 3650–3665.

Sugiyama, M., 2009: The Moisture Mode in the Quasi-Equilibrium Tropical Circulation Model. Part I: Analysis Based on the Weak Temperature Gradient Approximation. *J. Atmos. Sci.*, **66**, 1507–1523.

Trenberth, K. E., and D. P. Stepaniak, 2003: Covariability of components of poleward atmospheric energy transports on seasonal and interannual timescales. *Journal of climate*, **16 (22)**, 3691–3705.

Vallis, G. K., 2017: *Atmospheric and oceanic fluid dynamics*, Vol. 2. Cambridge University Press.

Windmiller, J. M., and G. C. Craig, 2019: Universality in the spatial evolution of self-aggregation of tropical convection. *Journal of the Atmospheric Sciences*, **76 (6)**, 1677–1696.

Wing, A. A., and K. A. Emanuel, 2014: Physical mechanisms controlling self-aggregation of convection in idealized numerical modeling simulations. *J. Adv. Model. Earth Syst.*, **6 (1)**, 59–74.

Wolding, B., J. Dias, G. Kiladis, F. Ahmed, S. W. Powell, E. Maloney, and M. Branson, 2020: Interactions between moisture and tropical convection. part i: The coevolution of moisture and convection. *Journal of the Atmospheric Sciences*, **77 (5)**, 1783–1799, https://doi.org/10.1175/JAS-D-19-0225.1.

Wolding, B. O., E. D. Maloney, and M. Branson, 2016: Vertically resolved weak temperature gradient analysis of the Madden-Julian Oscillation in SP-CESM. *J. Adv. Model. Earth Syst.*, https://doi.org/10.1002/2016MS000724.

Yanai, M., S. Esbensen, and J. Chu, 1973: Determination of bulk properties of tropical cloud clusters from large-scale heat and moisture budgets. *J. Atmos. Sci.*, **30**, 611–627, https://doi.org/10.1175/1520-0469(1973)030⟨0611:DOBPOT⟩2.0.CO;2.

Yasunaga, K., S. Yokoi, K. Inoue, and B. E. Mapes, 2019: Space–time spectral analysis of the moist static energy budget equation. *J. Climate*, **32 (2)**, 501–529, https://doi.org/10.1175/JCLI-D-18-0334.1.

Yu, J.-Y., C. Chou, and J. D. Neelin, 1998: Estimating the gross moist stability of the tropical atmosphere. *J. Atmos. Sci.*, **55 (8)**, 1354–1372, https://doi.org/10.1175/1520-0469(1998)055⟨1354:ETGMSO⟩2.0.CO;2.

Yu, J.-Y., and J. D. Neelin, 1994: Modes of Tropical Variability under Convective Adjustment and the Madden–Julian Oscillation. Part II: Numerical Results. *Journal of the Atmospheric Sciences*, **51 (13)**, 1895–1914, https://doi.org/10.1175/1520-0469(1994)051⟨1895:MOTVUC⟩2.0.CO;2.

Zhang, C., Á. F. Adames, B. Khouider, B. Wang, and D. Yang, 2020: Four theories of the madden-julian oscillation. *Reviews of Geophysics*, **58 (3)**, e2019RG000685, https://doi.org/10.1029/2019RG000685.